# A novel ion conducting route besides the central pore in an inherited mutant of G-protein-gated inwardly rectifying $K^+$ channel

I-Shan Chen[abc]*, Jodene Eldstrom[d], David Fedida[d], and Yoshihiro Kubo[ab]*

[a]Division of Biophysics and Neurobiology, Department of Molecular and Cellular Physiology, National Institute for Physiological Sciences, National Institutes of Natural Sciences, Okazaki 444-8585, Japan

[b]Department of Physiological Sciences, School of Life Science, SOKENDAI (The Graduate University for Advanced Studies), Hayama 240-0193, Japan

[c]Department of Pharmacology, School of Medicine, Wakayama Medical University, Wakayama 641-8509, Japan

[d]Department of Anesthesiology, Pharmacology and Therapeutics, University of British Columbia, Vancouver, British Columbia, V6T 1Z3, Canada

*Corresponding authors: I-Shan Chen, Yoshihiro Kubo

**Email:** chenis@wakayama-med.ac.jp; ykubo@nips.ac.jp

**ORCIDs:** I-S. C.: 0000-0003-3204-3921; J. E.: 0000-0002-7684-175X;
D. F.: 0000-0001-6797-5185; Y. K.: 0000-0001-6707-0837

**Preprint:** bioRxiv, DOI: https://doi.org/10.1101/2021.08.18.456735

**Abstract**

G-protein-gated inwardly rectifying $K^+$ (GIRK; Kir3.x) channels play important physiological roles in various organs. Some of the disease-associated mutations of GIRK channels are known to induce loss of $K^+$ selectivity but their structural changes remain unclear. In this study, we investigated the mechanisms underlying the abnormal ion selectivity of inherited GIRK mutants. By the two-electrode voltage-clamp analysis of GIRK mutants heterologously expressed in *Xenopus* oocytes, we observed that Kir3.2 G156S permeates $Li^+$ better than $Rb^+$, while T154del or L173R of Kir3.2 and T158A of Kir3.4 permeate $Rb^+$ better than $Li^+$, suggesting a unique conformational change in the G156S mutant. Applications of blockers of the selectivity filter (SF) pathway, $Ba^{2+}$ or Tertiapin-Q (TPN-Q), remarkably increased the $Li^+$-selectivity of Kir3.2 G156S but did not alter those of the other mutants. In single-channel recordings of Kir3.2 G156S expressed in mouse fibroblasts, two types of events were observed, one attributable to a TPN-Q sensitive $K^+$ current and the second a TPN-Q resistant $Li^+$ current. The results show that a novel $Li^+$ permeable and blocker-resistant pathway exists in G156S in addition to the SF pathway. Mutations in the pore helix (PH), S148F and T151A, also induced high $Li^+$ permeation. Our results demonstrate that the mechanism underlying the loss of $K^+$ selectivity of Kir3.2 G156S involves formation of a novel ion permeation pathway besides the SF pathway, which allows permeation of various species of cations.

## Introduction

G-protein-gated inwardly rectifying $K^+$ (GIRK) channels are stimulated by the activation of G-protein-coupled receptors (GPCRs) to regulate heartbeat, neuronal excitability and hormone secretion (Hibino et al., 2010). There are four types of GIRK subunits (Kir3.1, Kir3.2, Kir3.3, and Kir3.4) which form homotetramers of Kir3.2 or heterotetramers of multiple combinations in different tissues (Hibino et al., 2010; Krapivinsky et al., 1995; Kubo, Reuveny, Slesinger, Jan, & Jan, 1993; Lesage et al., 1994), and gene mutations encoded by GIRK channels have been found to cause diseases in some patients (Zangerl-Plessl, Qile, Bloothooft, Stary-Weinzinger, & van der Heyden, 2019). For example, deletion of Thr152, or mutations of Gly154 to Ser or Leu171 to Arg in the human Kir3.2 channel (encoded by *KCNJ6*), cause Keppen-Lubinsky syndrome (KPLBS) or KPLBS-like disorder (Horvath et al., 2018; Masotti et al., 2015), and G151R, T158A or L168R mutations in the human Kir3.4 channel (encoded by *KCNJ5)* cause aldosterone-producing adenomas (APA) (Boulkroun et al., 2012; Choi et al., 2011). These amino acid residues are conserved among GIRK subtypes. Some of the inherited mutations of these residues have been reported to cause loss of $K^+$ selectivity, resulting in disorder of cell function and cell death (Choi et al., 2011; Horvath et al., 2018; Navarro et al., 1996; Scholl et al., 2012; Slesinger et al., 1996).

$K^+$ selectivity is achieved by a highly conserved amino acid sequence TV(I)GYG which forms the selectivity filter (SF) in $K^+$ channels (Zagotta, 2006). Mutations in the SF sequence of $K^+$ channels alter ion selectivity (Heginbotham, Lu, Abramson, & MacKinnon, 1994). An ion pair, conserved in the Kir channel family, a glutamic acid located in the pore helix (PH) and an arginine located in the extracellular loop behind the SF, is known to contribute to stabilization of the pore structure and maintaining ion selectivity (Yang, Yu, Jan, & Jan, 1997). Mutations of other residues in the PH, such as Ser148 or Glu152 of mouse Kir3.2, also impair the $K^+$ selectivity (Chen et al.,

72 2019; Yi, Lin, Jan, & Jan, 2001). Mutations located in transmembrane domains (TMs)
73 outside the SF also alter ion selectivity and residues located at the central cavity can
74 also influence the ion selectivity through interaction with the permeating ions (Bichet,
75 Grabe, Jan, & Jan, 2006; Bichet et al., 2004; Matamoros & Nichols, 2021; Yi et al.,
76 2001). Structures of various types of $K^+$ channel have been identified by Cryo-EM
77 and X-ray crystallography (Long, Campbell, & Mackinnon, 2005; Miller & Long, 2012;
78 W. Wang & MacKinnon, 2017; Whorton & MacKinnon, 2011). However, the structural
79 changes induced by mutations at different regions of the channel which alter the ion
80 selectivity still remain to be elucidated.

81 Previous studies using homology modeling have predicted structural changes to
82 GIRK channels induced by disease associated mutations as follows: (A) mutations in
83 the SF (human Kir3.2 T152del or Kir3.2 G154S) impair the stabilization of $K^+$
84 interaction with the backbone of the SF (Masotti et al., 2015); (B) the L171R mutation
85 in the TM2 of human Kir3.2 limits the SF movement by the formation of a hydrogen
86 bond with Glu148 in the PH (Horvath et al., 2018), while the L168R mutation at the
87 corresponding position of human Kir3.4 is relevant to the interaction with the side
88 chain of Tyr of the GYG motif in the SF (Choi et al., 2011); (C) the T158A mutation in
89 the extracellular loop of human Kir3.4 weakens the stability of the structure by
90 eliminating the hydrogen bonds between the extracellular loop, PH, and TM1 (Choi et
91 al., 2011). However, no further experimental data have been provided to support
92 these hypotheses.

93 In the present study, we investigated the mechanisms underlying the abnormal ion
94 selectivity of these inherited mutations in Kir3.2 and Kir3.4 channels by introducing
95 mutations at the corresponding positions in mouse Kir3.2 or rat Kir3.4. Using
96 electrophysiological recordings in *Xenopus* oocytes, we demonstrate that most of
97 these mutations induce a conformational change which allows increased permeation
98 of $Rb^+$ or $Cs^+$, while the G156S mutation of the Kir3.2 channel (corresponding to

human Kir3.2 G154S) induces a different conformational change which allows better permeation of $Li^+$ or $Na^+$ over $Rb^+$ or $Cs^+$. Applications of pore blockers of GIRK channels increase the $Li^+$-selectivity of Kir3.2 G156S but do not influence that of the other mutants. Single-channel recordings of the G156S mutant in mouse fibroblasts show that two types of ion conducting events, which respectively reflect $K^+$ current via the SF pathway and $Li^+$ current via a novel ion permeation pathway, exist in the same recording. Mutations of amino acid residues located in the PH behind the SF also gave rise to the $Li^+$-permeable pathway outside of the SF route. Our results reveal a novel mechanism underlying the loss of $K^+$-selectivity of Kir3.2 G156S that involves formation of a novel ion permeation pathway in addition to the conventional SF route.

## Results

### Different disease associated mutations of GIRK channels show diverse ion selectivity

To characterize the ion selectivity changes of GIRK channels induced by inherited mutations, we constructed these mutants using mouse Kir3.2 or rat Kir3.4 channels (Figure 1a). These mutants were heterologously expressed in *Xenopus* oocytes and the ionic currents were recorded by two-electrode voltage-clamp. We first recorded the $K^+$ current with an extracellular solution containing 96 mM $K^+$, and then replaced the $K^+$ with other cations. The order of their ionic size is $Li^+ < Na^+ < K^+ < Rb^+ < Cs^+ <$ methylammonium$^+$ ($MA^+$) < tetramethylammonium$^+$ ($TMA^+$) < tetraethylammonium$^+$ ($TEA^+$) < n-methyl-d-glucamine$^+$ ($NMDG^+$).

By using a ramp voltage pulse from -100 mV to +40 mV, we observed that wild-type (WT) Kir3.2 showed a large $K^+$ current and a minor $Rb^+$ current at -100 mV (Figure 1b). Only negligible currents were observed when $K^+$ was replaced with other cations. The current amplitude of each cation ($I_X$) at -100 mV relative to that of $K^+$ ($I_K$) is referred to as $I_X$ / $I_K$ in Figure 1c. To analyze the ion selectivity quantitatively, the change of the reversal potentials by replacing the extracellular cations is usually used. In the case of GIRK channels which show strong rectification, however, the reversal potential is significantly affected by even a small leak current which hinders accurate analysis of $P_X$ / $P_K$. Isolation of the GIRK current component by using blockers was also not possible, due to the decreased sensitivity to pore blockers as shown in Figures 2, 3, 6 and 7. Thus, we did not perform the measurement of the reversal potential in this study except for those in Figure 3 h-j. We instead compared the current amplitude in various extracellular solutions. The information we present in this study to compare the ion selectivity is the profile of sequence of current amplitudes which reflects the extent of the permeation of various ions.

137 Deletion of Kir3.2 Thr154 in the SF resulted in inward currents induced by various
138 extracellular cations in the order of $K^+$ > $Rb^+$ > $Na^+$ > $Li^+$ ≈ $Cs^+$ ≈ $MA^+$ (Figure 1d, e).
139 Mutation of Kir3.2 Gly156 in the SF to Ser also showed abnormal inward currents but
140 the sequence of current amplitudes produced by various cations was different from
141 that of T154del (Figure 1f, g). Kir3.2 G156S showed larger $Na^+$, $Li^+$, $MA^+$ currents
142 than $Rb^+$ or $Cs^+$ currents. Since the homotetramers of the Kir3.4 SF mutant G151R
143 showed very small currents from all extracellular cations, ion permeation could not be
144 compared because of contamination from endogenous currents (Figure 1-figure
145 supplement 1a). We, therefore introduced the mutation at the corresponding position
146 of Kir3.2 (G156R) and observed that its ion selectivity was different from that of
147 Kir3.2 G156S (Figure 1f-i). G156R showed a high selectivity to $Rb^+$, $Cs^+$ and $MA^+$,
148 and less inward rectification. The results show that mutation of Gly156 to different
149 amino acid residues induces distinct conformational changes to the ion permeation
150 pathway.
151 Kir3.4 T158A (T163A in Kir3.2; Figure 1a) in the extracellular loop after the SF also
152 showed an abnormal ion selectivity (Figure 1-figure supplement 1b, c) which was
153 similar to those of G156R and L173R in the TM2 of Kir3.2 (Figure 1a, h, i, l, m). A
154 previous study suggested that this may be relevant to the eliminated hydrogen bonds
155 of Thr158 with Pro128, Cys129 and Lys160, which are conserved among GIRK
156 subtypes (Choi et al., 2011). However, when we introduced the corresponding
157 mutation into Kir3.2 in the extracellular loop after the SF (T163A), it showed an intact
158 ion selectivity and inward rectification like the WT (Figure 1b, c, j, k). This suggests
159 that the hydrogen bonds formed between the threonine and the three conserved
160 residues are not necessarily relevant to the ion selectivity change. Instead, the
161 extracellular loop may play some roles to maintain the ion selectivity.
162 Essentially, no significant currents were observed in the WT and all mutants when
163 replacing the extracellular cations with $TMA^+$, $TEA^+$ or $NMDG^+$ (Figure 1 and Figure

164 1-figure supplement 1b, c), showing that these mutants did not allow the permeation
165 of extra-large cations. These results demonstrate that most of the inherited mutations
166 of Kir3.2 or Kir3.4 channels induce a conformational change with higher $Rb^+$ and $Cs^+$
167 permeability than for $Na^+$ and $Li^+$. However, a unique conformational change is
168 induced by the G156S mutation of Kir3.2 with higher permeation of $Na^+$ and $Li^+$ than
169 $Rb^+$ and $Cs^+$.
170
171 **Effect of $Ba^{2+}$ on the ion selectivity of Kir3.2 G156S**
172 To further characterize the property of ion permeation for each mutant, we examined
173 the effect on ion selectivity of a well-established pore blocker of Kir channels, $Ba^{2+}$.
174 $Ba^{2+}$ is known to block the ion permeation pore of Kir channels by strong interaction
175 with the threonine residue located at the bottom of the SF (eg. Thr154 in Kir3.2)
176 (Alagem, Dvir, & Reuveny, 2001; Hsieh, Kuo, & Huang, 2015). We first investigated
177 the potency and efficacy of $Ba^{2+}$ in the inhibition of $K^+$ currents for WT and mutants of
178 Kir3.2. Application of $Ba^{2+}$ inhibited the $K^+$ current of WT, G156S and T163A well
179 ($IC_{50}$: 105 ± 19 μM for WT; 95 ± 37 μM for G156S; 78 ± 11 μM for T163A, n = 5 for
180 each), and inhibited T154del with an intermediate potency (Figure 2a-g). The
181 sensitivity of G156R and L173R to the block by $Ba^{2+}$ was very low. Kir3.4 T158A also
182 showed a very low sensitivity to $Ba^{2+}$ (Figure 2-figure supplement 1a, b).
183 We next examined the ion selectivity of mutants before and after the application of
184 a high concentration of $Ba^{2+}$ (3 mM), except Kir3.2 WT and the WT-like mutant
185 T163A. For T154del, G156R, L173R of Kir3.2 or T158A of Kir3.4, application of $Ba^{2+}$
186 did not influence the sequence of $I_X/I_K$ of cations tested (Figure 2h, i, l-o and Figure 2-
187 figure supplement 1c, d). Unexpectedly, $Ba^{2+}$ did change the sequence of ion
188 selectivity of Kir3.2 G156S, which showed an apparent increase in the $I_{Li}/I_K$, $I_{Na}/I_K$ and
189 $I_{MA}/I_K$ (Figure 2j, k). The current amplitude of $Li^+$, $Na^+$ or $MA^+$ at -100 mV became
190 larger than the $K^+$ current in the presence of $Ba^{2+}$. These results show that Kir3.2

191 G156S possesses a different ion permeation mechanism from that of the other
192 mutants.
193 We examined the dose-inhibition relationship of $Ba^{2+}$ on the $K^+$ and the $Li^+$ currents
194 of Kir3.2 G156S (Figure 2p). The curve was shifted to the right when extracellular $K^+$
195 was replaced with $Li^+$, suggesting that $Ba^{2+}$ blocks the $Li^+$ permeation with a lower
196 affinity than that of the $K^+$ permeation. There are two possible explanations for the
197 altered permeation and block of the G156S mutant as follows. (1) On top of the SF
198 pathway blocked by $Ba^{2+}$ with a high affinity, a novel ion permeation pathway is
199 formed which allows permeation of $Li^+$, $Na^+$ and $MA^+$ with a lower sensitivity to the
200 block by $Ba^{2+}$. (2) $Ba^{2+}$ firmly binds to the threonine (Thr154) at the bottom of SF
201 when $K^+$ ions enter the SF, while the $Ba^{2+}$ binding becomes unstable when $Li^+$, $Na^+$ or
202 $MA^+$ enter the SF pathway.
203
204 **Effect of TPN-Q on the ion selectivity of Kir3.2 G156S**
205 To further clarify whether a novel ion permeation pathway besides the conventional
206 SF route does exist in Kir3.2 G156S, we examined the effect of another pore blocker
207 which binds to the GIRK channel at a different position than $Ba^{2+}$. Here we used
208 Tertiapin-Q (TPN-Q) known to specifically block Kir1.1 and GIRK channels by
209 capping the SF pore from the extracellular side (Figure 3a) (Doupnik, Parra, & Guida,
210 2015; Patel, Kuyucak, & Doupnik, 2020). Application of TPN-Q inhibited the $K^+$
211 current strongly and inhibited the $Li^+$ current weakly in Kir3.2 G156S (Figure 3b-d). In
212 the presence of TPN-Q, $Li^+$, $Na^+$ or $MA^+$ current at -100 mV became approximately 5-
213 10 times larger than the $K^+$ current (Figure 3e, f). The $I_{Li}/I_K$, $I_{Na}/I_K$ and $I_{MA}/I_K$ were
214 increased by the application of TPN-Q, and this is consistent with the effect of $Ba^{2+}$
215 application (Figure 3f and 2k). We calculated the percent inhibition of the current for
216 each cation and found that 1 μM of TPN-Q inhibited about 83~90% of the $K^+$, $Rb^+$, or
217 $Cs^+$ currents, 52.9 ± 9.3 % of the $Na^+$ current, 47.8 ± 7.9 % of the $MA^+$ current, and

218 30.1 ± 7.2 % of the $Li^+$ current (n = 5 for each, Figure 3g). One possible interpretation
219 of the results would be as follows: $K^+$, $Rb^+$, or $Cs^+$ predominantly permeate through
220 the channel via the SF pathway, with a very a limited permeation via the novel route;
221 in the case of $Na^+$ or $MA^+$, half and half permeation occurs through the two pathways;
222 $Li^+$ permeates predominantly through the novel route which is less sensitive to the
223 block by TPN-Q.
224 To clarify whether a novel permeation pathway with a high $Li^+$-permeability does
225 exist in Kir3.2 G156S in addition to the SF route with a high $K^+$-permeability, we
226 examined the permeability of $Li^+$ ($P_{Li}$) relative to the permeability of $K^+$ ($P_K$) by
227 measuring the shift of reversal potentials ($\Delta E_{rev}$) upon replacement of the
228 extracellular $Li^+$ with the same concentration of $K^+$ (Figure 3h-j). In the absence of
229 TPN-Q, $E_{rev}$ of $Li^+$ current was -2.7 ± 5.8 mV (n = 5) and was shifted to the right in K+
230 solution (8.1 ± 5.4 mV, n = 5), showing that $P_K$ is larger than $P_{Li.}$ $E_{rev}$ of the $K^+$ current
231 shifted to the left on application of 1 μM TPN-Q (-9.6 ± 11.1 mV, n = 5) and shifted to
232 the right upon replacement of $K^+$ with $Li^+$ (-1.2 ± 6.3 mV, n = 5), showing that $P_K$ was
233 decreased by TPN-Q and that $P_K$ is smaller than $P_{Li}$ in the presence of TPN-Q. Taken
234 together, when the SF pathway was blocked by TPN-Q, a high $P_{Li}/P_K$ was observed
235 presumably due to the novel ion permeation route. When the SF route is not blocked,
236 a lower $P_{Li}/P_K$ was observed as a result of the presence of two pathways.
237
238 **Activation effect of $G_{\beta\gamma}$ and Ivermectin on Kir3.2 G156S**
239 Previous studies showed that heteromeric channels comprised of Kir3.2 G156S and
240 Kir3.1 are insensitive to $G_{\beta\gamma}$-stimulation (Navarro et al., 1996). Here we examined
241 whether homomeric channels of Kir3.2 G156S are also insensitive to the $G_{\beta\gamma}$-
242 stimulation by coexpressing Kir3.2 G156S with the muscarinic M2 receptor (M2R).
243 We observed that an application of 1 μM ACh increases the $K^+$ current of Kir3.2 WT
244 but does not apparently increase that of G156S (Figure 4), showing that

245 homotetramers of Kir3.2 G156S are also insensitive to $G_{\beta\gamma}$-stimulation as compared
246 with the WT. We also examined the effect of another activator of Kir3.2 channels,
247 Ivermectin (IVM), which directly interacts with the channel as we reported previously
248 (Chen & Kubo, 2018; Chen, Tateyama, Fukata, Uesugi, & Kubo, 2017). Applications
249 of 10 μM IVM induced the current increase in both the Kir3.2 WT and G156S mutant.
250 This shows that the limited response of the G156S mutant to ACh stimulation is not
251 due to the high basal activity reaching a saturation level, since IVM can further
252 increase the current amplitude. Taken together, the G156S mutation may induce a
253 conformational change that occurs not only in the SF region but also in the structural
254 components which play roles in the $G_{\beta\gamma}$-coupling-channel activation linkage.
255

256 **Single-channel recordings of Kir3.2 G156S show two types of ion conducting**
257 **events**

258 We speculated that there should be two types of ion conducting events in G156S,
259 one generated by $K^+$ permeation through the SF route and the other generated by $Li^+$
260 permeation through the novel route. To verify this hypothesis, we performed cell-
261 attached single-channel recordings using mouse fibroblasts heterologously
262 expressing Kir3.2 G156S with a pipette solution of 140 mM $K^+$, 140 mM $Li^+$, or a
263 mixture of 70 mM $K^+$ and 70 mM $Li^+$, in the absence or presence of TPN-Q
264 respectively (Figure 5). In 140 mM $K^+$ at -100 mV, we observed inward currents with
265 amplitudes up to ~2 pA (Figure 5a). When 400 nM TPN-Q was added to the pipette
266 solution, these events with a relatively large current amplitude were largely absent
267 and replaced by infrequently observed events with a very small current amplitude (<
268 0.2 pA) (Figure 5b). Occasional amplifier resets were unavoidable during these long
269 recordings due to the need to reset the headstage output periodically as part of the
270 capacitive feedback system used to achieve low noise recordings (Figure 5b). The

271 results demonstrate that the major events of larger conductance by $K^+$ influx of Kir3.2
272 G156S were blocked by TPN-Q (Figure 5g).
273 In 140 mM $Li^+$, inward current events with a peak amplitude smaller than 1 pA were
274 recorded (Figure 5c), smaller than those observed in 140 $K^+$ in Figure. 5a. Inclusion
275 of 400 nM TPN-Q in the pipette did not apparently change the activity and the
276 amplitude of $Li^+$ current (Figure 5c, d), showing that the major events caused by $Li^+$
277 influx through Kir3.2 G156S were not blocked by TPN-Q (Figure 5g).
278 To clarify whether the $K^+$ conducting events and $Li^+$ conducting events are present
279 in the same recording, we performed recordings with 70 mM $K^+$ and 70 mM $Li^+$
280 solution in the pipette. In the current recordings with a slow ramp pulse from +30 mV
281 to -150 mV for 40 s, the conductance was reduced by the presence of 400 nM TPN-
282 Q in the pipette, at the tested membrane potentials (Figure 5-figure supplement 1). In
283 the current recordings held at -100 mV in the absence of TPN-Q, two types of inward
284 current events were detected; one type of event with a peak amplitude > 0.5 pA and
285 another type of event with a peak amplitude < 0.5 pA (Figure 5e). The events with a
286 larger amplitude between 4 s and 5 s in Figure. 5e were interpreted to be the sum of
287 simultaneous activities of two type of events. In the presence of 400 nM TPN-Q, only
288 the smaller events with < 0.5 pA remained (Figure 5f), and similar events were also
289 observed in Figure. 5e between 5 s and 6 s. These data together with those in Figure
290 5a-d suggest that the single channel events with a larger amplitude blocked by TPN-
291 Q involve $K^+$ influx, and the events with a smaller amplitude which remained in the
292 presence of TPN-Q involve $Li^+$ influx. These results demonstrate that two types of ion
293 conducting events are present in the same recording of Kir3.2 G156S. This supports
294 that a novel ion permeation pathway in addition to the SF route is formed by the
295 G156S mutation in the Kir3.2 channel.
296

297 **Mutations in the pore helix located behind the SF also form a $Li^+$-permeable**
298 **pathway**
299 To reveal the location of the novel ion permeation route, we introduced a point
300 mutation into the PH located behind the SF, since there is a pocket accessible from
301 the extracellular side surrounded by the side chains of amino acid residues of the SF
302 and PH in the WT. We previously reported that the S148F mutant located at the
303 center of the PH in Kir3.2 is $Na^+$-permeable (Chen et al., 2019) (Figure 6a). Here we
304 examined the ion permeation of various cations and observed that this mutant
305 permeates $Li^+$, $Na^+$, $Rb^+$, $Cs^+$ and $MA^+$ and their $I_X/I_K$ are 0.92 ± 0.04 for $MA^+$ and
306 about 0.43~0.60 for the other cations (n = 6 for each, Figure 6b, d). The dose-
307 inhibition relationship for Kir inhibitors on Kir3.2 S148F showed that 3 mM $Ba^{2+}$
308 blocks 72.8 ± 3.9 % of the $K^+$ current and 1 μM TPN-Q blocks 48.0 ± 16.0 % (n = 5
309 for each, Figure 6c). In the presence of $Ba^{2+}$ or TPN-Q, the $I_{Li}/I_K$, $I_{Na}/I_K$, and $I_{MA}/I_K$
310 became larger than those in the absence of these inhibitors (Figure 6d),
311 demonstrating that a novel route, which is permeable to $Li^+$, $Na^+$ and $MA^+$ and
312 insensitive to the block by TPN-Q, exists also in the S148F mutant.
313 Unexpectedly, mutation of Thr151, which is located at the bottom of the PH (Figure
314 7a), to Ala induced an extremely high rate of $Li^+$ permeation, even in the absence of
315 SF route blockers (Figure 7b). The $K^+$ current of Kir3.2 T151A was very small and the
316 $Li^+$, $Na^+$ and $MA^+$ currents were far larger than the $K^+$ current ($I_{Li}/I_K$: 19.1 ± 9.2; $I_{Na}/I_K$:
317 11.8 ± 6.1; $I_{MA}/I_K$: 17.7 ± 7.2, n = 10 for each) (Figure 7b, d). The T151C mutation also
318 showed high $I_{Na}/I_K$ ($I_{Na} > I_K$). However, only a limited number of successful recordings
319 were obtained, due to the very unhealthy condition of the oocytes expressing the
320 T151C mutant (Figure 7-figure supplement 1). Mutation of Thr151 to Ser retained
321 intact $K^+$ selectivity as WT, while mutation of Thr151 to Asp, Asn, Lys, Tyr, or Phe
322 triggered permeation of $Na^+$, but $I_{Na}$ was still smaller than $I_K$ (Figure 7-figure
323 supplement 1b). Oocytes expressing other T151 mutants showed very small currents

324 (Figure 7-figure supplement 1a). These results show that the Ala mutant at this
325 position increases the $Na^+$, $Li^+$ permeation. Since the $K^+$ current of the T151A mutant
326 was very tiny, hindering detailed dose-inhibition relationship analysis, we compared
327 the inhibiting effect of blockers on the $Li^+$ current (Figure 7c). Application of 3 mM
328 $Ba^{2+}$ blocked 59.5 ± 6.0 % (n = 5) of the $Li^+$ current and 1 μM TPN-Q only slightly
329 reduced the $Li^+$ current (10.1 ± 2.5 %, n = 5, Figure 7c). The sequence of $I_X/I_K$ did not
330 change apparently by applying blockers (Figure 7d), suggesting that T151A mutant
331 has only a novel ion permeation pathway. The results demonstrate that this ion
332 permeation route allows $Li^+$, $Na^+$ and $MA^+$ permeation better than $K^+$ or $Rb^+$, and is
333 insensitive to the block by TPN-Q. These are consistent with the features of the novel
334 pathway identified in Kir3.2 G156S. It appears that the T151A mutation induces a
335 conformational change which forms a $Li^+$-permeable pathway in the pocket
336 surrounded by the SF and PH residues, that the SF route is collapsed to inhibit $K^+$
337 permeation, and that $Ba^{2+}$ enters the novel ion permeation pathway and inhibits $Li^+$
338 current with a lower binding affinity than that for the SF route in WT (Figure 7a). This
339 is similar to the dose-inhibition curve for $Ba^{2+}$ on the $Li^+$ currents of Kir3.2 G156S, that
340 is shifted to the right compared to that of the $K^+$ current (Figure 2p).
341 During the recordings, we observed that the T151A mutant shows a very slow
342 current increase or decrease when exchanging extracellular $K^+$ to $Na^+$ or $Na^+$ to $K^+$ as
343 compared with the Kir3.2 WT (Figure 7-figure supplement 2). However, when we
344 exchanged the extracellular $Na^+$ to the impermeable $NMDG^+$ or $NMDG^+$ to $Na^+$, the
345 current change kinetics of T151A were as fast as those in WT. This suggests that the
346 cations, which occupy the novel pathway, might strongly interact with the pathway
347 lining residues.
348
349

350 **Discussion**

351 We have presented the following in this study: (1) Kir3.2 G156S permeates $Li^+$ and
352 $Na^+$ better than $Rb^+$ and $Cs^+$, while the other inherited mutants of GIRK channels
353 permeate $Rb^+$ and $Cs^+$ better than $Li^+$ and $Na^+$ (Figure 1); (2) applications of SF pore
354 blockers increase the $Li^+$ and $Na^+$-selectivity of Kir3.2 G156S but do not alter those of
355 the other mutants (Figures 2 and 3); (3) single-channel recordings of Kir3.2 G156S
356 show events of $K^+$ influx which are blocked by extracellular TPN-Q, and also those of
357 $Li^+$ influx which are not blocked by TPN-Q (Figure 5); (4) Kir3.2 S148F also shows an
358 increased $Li^+$-selectivity in the presence of pore blockers (Figure 6); (5) Kir3.2 T151A
359 shows an extremely high $Li^+$-selectivity which is not influenced by the application of
360 pore blockers (Figure 7).

361 Our results demonstrate that a novel ion permeation pathway allowing $Li^+$, $Na^+$, or
362 $MA^+$ influx is formed in Kir3.2 G156S, besides the conventional central pore route
363 formed by the SF which is blocked by $Ba^{2+}$ or TPN-Q (Figures 2k and 3f). This novel
364 ion permeation route is similar to a side entry pathway for $Na^+$ permeation through
365 the sodium potassium (NaK) channel (Roy et al., 2021; Shi et al., 2018). The SF of
366 the NaK channel is constructed by TVGDG, with D66 diverging from the conserved
367 SF sequence of $K^+$ channels. NaK channels permeate $K^+$ in a symmetric
368 conformation of the SF, while another asymmetric conformation of the lower part of
369 the SF, composed of different subunits, is necessary for $Na^+$ conduction (Shi et al.,
370 2018). When D66 of the SF flips, $Na^+$ associates with the side entry binding site
371 behind the SF pore (Roy et al., 2021). $K^+$ was also shown to associate with the side
372 entry binding site, in addition to the canonical $K^+$ binding sites within the SF (Roy et
373 al., 2021). In our single-channel recordings of G156S, $K^+$ conducting events with a
374 tiny current amplitude were infrequently observed in the presence of TPN-Q (Figure
375 5b), suggesting that $K^+$ may also slightly permeate through the novel ion permeation
376 route of Kir3.2 G156S. Mutants of the voltage-gated $K^+$ channel, Kv1.2 V370C or

377 Kv1.3 V388C, are also suggested to possess an unconventional cation permeation
378 pathway, named the σ-pore behind the SF pore, which permeates cations in a
379 sequence of efficacy of $Li^+$ > $Na^+$ > $NH_4^+$ > $Cs^+$ > $K^+$ > $Rb^+$ (Prutting & Grissmer, 2011;
380 Tyutyaev & Grissmer, 2017, 2018). The reported $Li^+$-preferable permeation of the σ-
381 pore is consistent with the feature of the novel ion permeation pathway which we
382 have identified in Kir3.2 G156S.

383 The G156S mutation of mouse Kir3.2 causes the loss of cerebellar granule cells in
384 *weaver* mice (Patil et al., 1995). Blocking of $Na^+$ flux through *weaver* Kir3.2 channels
385 by MK-801 and QX-314 at the early stage of development is known to rescue the
386 survival and differentiation of *weave*r granule neurons (Kofuji et al., 1996). The
387 inherited mutations of human Kir3.4, G151R and L168R which correspond to Gly156
388 in the SF and Leu173 in the TM2 of mouse Kir3.2, are reported to increase
389 aldosterone synthesis (Choi et al., 2011; Velarde-Miranda, Gomez-Sanchez, &
390 Gomez-Sanchez, 2013). Macrolides inhibits these mutants but not the WT channel,
391 and potentially serves as a diagnostic tool for APA patients harboring these
392 mutations (Maiolino et al., 2018; Scholl et al., 2017). We observed that the Kir3.2
393 G156R mutant shows a $Rb^+$, $Cs^+$-preferable permeation which is insensitive to block
394 by $Ba^{2+}$ (Figure 2). This is different from the features of Kir3.2 G156S, which is $Na^+$,
395 $Li^+$-preferable and $Ba^{2+}$-sensitive, suggesting that mutations of Gly156 to different
396 amino acid residues induced distinct conformational changes in the permeation
397 pathway. Kir3.2 L173R also showed $Rb^+$, $Cs^+$-preferable and $Ba^{2+}$-insensitive
398 features like that of Kir3.2 G156R. This may be due to the dilated SF in these
399 mutants that underlies the nonselective conformation of the SF with reduced
400 sensitivity to the $Ba^{2+}$ block, as suggested in a study of KirBac1.1 using single-
401 molecule FRET analysis (S. Wang et al., 2019).

402 The $Ba^{2+}$ blockade in a $Ca^{2+}$-activated $K^+$ channel, MthK, is known to be modulated
403 by extracellular cations (Guo, Zeng, Cui, Chen, & Ye, 2014). There are four hydrated

404 $K^+$-binding sites (S1~S4) in the SF of $K^+$ channels (Doyle et al., 1998; Zhou, Morais-
405 Cabral, Kaufman, & MacKinnon, 2001). When the MthK channel pore is filled with $K^+$,
406 $Ba^{2+}$ blocks ion permeation by staying at the S3 and S4 sites predominantly, while
407 $Ba^{2+}$ stays at the S2 site in a $Na^+$ environment, which weakens the block (Guo et al.,
408 2014). Therefore, it is possible that the $Ba^{2+}$ block of Kir3.2 G156S in different
409 extracellular cation environments could be different, resulting in the increase of $I_X/I_K$
410 in the presence of $Ba^{2+}$ (Figure 2). However, this possibility is unlikely, because
411 another inhibitor TPN-Q, which blocks the pore without entering the SF, but by
412 capping the pore instead, also shows similar increases of $I_X/I_K$ for the same type of
413 cations in Kir3.2 G156S (Figures 2k and 3f). These results suggest that the alteration
414 of the ion selectivity by application of blockers is unlikely to be due to the modulation
415 of blocker binding in the SF pore by extracellular cations. A similar phenomenon was
416 also observed in Kir3.2 S148F (Figure 6), further supporting that a $Li^+$-permeable
417 pathway which is not blocked by $Ba^{2+}$ or TPN-Q, exists in Kir3.2 G156S and S148F
418 mutants. We previously introduced various amino acid residues at the S148 position
419 in Kir3.2 and found that a nonpolar and bulky side chain at this position make the
420 channel permeable to $Na^+$ (Chen et al., 2019). We also demonstrated that T151A in
421 the PH contributes to the formation of the $Na^+$, $Li^+$-conducting route behind the SF
422 (Figure 7), suggesting important roles of PH residues in the modulation of ion
423 selectivity.
424 Based on the sequence of permeation for various ions and the presence or
425 absence of sequence change by application of blockers, it was shown that G156S
426 (Figures 2k and 3f) and S148F (Figure 6d) of Kir3.2 both have the modified SF route
427 which permeates $Rb^+$ and $Cs^+$ well and the novel pathway which permeates $Li^+$ and
428 $Na^+$ preferably. It was also shown that T151A has only the novel pathway (Figure 7d),
429 whereas T154del (Figure 2i), G156R (Figure 2m) and L173R (Figure 2o) of Kir3.2
430 have only the modified SF pathway. The sequence of ion preference of the G156R

431 and L173R mutants ($Rb^+$, $Cs^+$-preferable permeation) fits to I – IV of the Eisenman
432 sequence, suggesting that the modified SF pathway is a weak-field-strength site
433 type, where the site-interaction energy is less than the hydration energy (Eisenman,
434 1962; Hille, 2001). In the case of the G156S mutant, the sequence of ion preference
435 in the absence of blockers does not fit to any of the Eisenman sequences, further
436 supporting the current is a mixture via multiple pathways. However, G156S in the
437 presence of blockers or T151A in the absence/presence of blockers, show ion
438 preferences which fit to XI or X of the Eisenman sequences, suggesting that the
439 novel ion permeation pathway is a strong-field-strength site type, where the site-
440 interaction energy overwhelms the hydration energy (Eisenman, 1962; Hille, 2001).
441 The slow kinetics of current amplitude change of T151A upon the exchange of
442 extracellular cations also supports the strong interaction of ions with their binding
443 sites (Figure 7-figure supplement 2). It is likely that the novel pathway is located in
444 the pocket between the PH and side chain of the SF, behind the central SF, and
445 further studies are needed to elucidate the detail of the whole route.
446 We observed in the single channel recording analysis of Kir3.2 G156S in $K^+$ and $Li^+$
447 that there are two types of events, a larger one presumably carried by $K^+$, sensitive to
448 the block by TPN-Q and a smaller one, presumably carried by $Li^+$, resistant to the
449 TPN-Q block (Figure 5e, f). If permeation through both pathways is independent and
450 allow permeation simultaneously, it is naturally expected the sum height of two types
451 of single channel events would be observed. At 4 s - 5 s of the recording in Figure
452 5e, larger events were observed, which could be an indication of overlapping
453 activities of both types. Further detailed analysis was not performed due to the
454 difficulty of the precise estimation of the small current amplitudes of fast gating
455 events. It may be natural to expect that there will be four novel side pathways behind
456 the SF in one tetrameric channel. If this is the case, multiple levels of single channel
457 current amplitudes might be observed. However, due to the relatively low open

458 probability, the multiple levels of overlapped activities could not be clearly observed.
459 Thus, a conclusion as to the number of novel pathways in one tetramer could not be
460 drawn.
461 In conclusion, our results reveal the presence of a novel ion permeation pathway
462 besides the SF route in Kir3.2 G156S. This provides us with novel insight into the
463 mechanisms underlying the loss of $K^+$ selectivity induced by inherited mutations in
464 GIRK channels. The design of drugs that selectively block the novel cation
465 permeation route alone to eliminate the abnormal cation fluxes may have the
466 potential to develop a novel treatment for Kir disorders such as for KPLBS patients
467 with the Kir3.2 G154S mutation (corresponding to mouse G156S) at an early stage of
468 life.
469

470 **Materials and Methods**

471

472 **Ethical approval of animal experiments**

473 All animal experiments in this study were approved by the Animal Care Committee of
474 the National Institutes of Natural Sciences (an umbrella institution of National Institute
475 for Physiological Sciences, Japan), and were performed in accordance with its
476 guidelines.

477

478 **Mutagenesis and cRNA preparations**

479 We constructed mutants of Kir3.2 and Kir3.4 and prepared their cRNA as described
480 previously (Chen et al., 2019). By PCR using PfuUltra II Fusion HS DNA Polymerase
481 kit (Agilent technologies, Santa Clara, CA, USA) and the primers (Supplementary
482 Table 1), we introduced point mutations in mouse Kir3.2 (GenBank accession no.:
483 AF040051) or rat Kir3.4 (GenBank no.: L35771) which were confirmed by DNA
484 sequencing. Their cDNA were linearized by restriction enzymes, and the
485 complementary RNA were transcribed by the mMessage T3 or T7 mMachine Kit
486 (Ambion, Austin, TX, USA). The cRNA of Kir3.2 (25 ng oocyte$^{-1}$ for the wild-type,
487 T154del, G156R or T163A; 5 ng oocyte$^{-1}$ for L173R or T151A; 0.5 ng oocyte$^{-1}$ for
488 G156S or S148F), Kir3.4 (25 ng oocyte$^{-1}$ for the G151R or T158A), and porcine
489 muscarinic M2 receptor (M2R, GenBank no.: X04708, 5 ng oocyte$^{-1}$) were injected
490 into *Xenopus* oocytes.

491

492 **Oocyte preparations**

493 We purchased adult female *Xenopus laevis* from Hamamatsu Seibutsu Kyouzai
494 (Hamamatsu, Japan). Isolation of oocytes from the frogs were performed as
495 described previously (Chen et al., 2019). Frogs were anaesthetized with 0.15%
496 tricaine (Sigma-Aldrich, St. Louis, MO, USA) for 30 min and then the oocytes were

497 dissociated by making an incision in the abdomen. Oocytes were treated with 2 mg
498 $ml^{-1}$ collagenase type I (Sigma-Aldrich) for 6 hours in frog Ringer's solution containing
499 (mM): 88 NaCl, 1 KCl, 2.4 $NaHCO_3$, 0.3 Ca $(NO_3)_2$, 0.41 $CaCl_2$, 0.82 $MgSO_4$, and 15
500 HEPES, pH 7.6 with NaOH. After removing the follicles, each oocyte was injected
501 with 50 nl of cRNA solution and then incubated in frog Ringer's solution with 0.1%
502 penicillin-streptomycin (Sigma-Aldrich) at 17°C. The oocytes were used for two-
503 electrode voltage-clamp recordings 1-5 days after the injection of cRNA.
504

505 **Two-electrode voltage-clamp recordings**

506 Glass electrodes for two-electrode voltage-clamp recordings had a resistance of 0.2-
507 0.5 MΩ when filled with a pipette solution containing 3 M potassium acetate and 10
508 mM KCl. Membrane currents of oocytes were recorded at 22-25°C in a high $K^+$
509 solution containing (mM): 96 KCl, 3 $MgCl_2$, and 5 HEPES, pH 7.3 with n-methyl-d-
510 glucamine (NMDG). To evaluate the ion selectivity, the KCl was replaced by LiCl,
511 NaCl, RbCl, CsCl, methylammonium-Cl, tetramethylammonium-Cl,
512 tetraethylammonium-Cl, or NMDG-Cl, one at a time. Data were recorded by an
513 oocyte clamp amplifier OC-725C (Warner instruments, Holliston, MA, USA), a digital
514 converter Digidata 1440 (Molecular devices, San Jose, CA, USA), and pCLAMP 10
515 software (Molecular devices). Compounds were applied to the extracellular solution
516 and perfused the oocytes in a recording chamber. Sequential applications of blockers
517 to the extracellular solution were performed and the recording data were fitted to a
518 Hill equation to acquire the dose-inhibition relationship as follows:
519 $y = min + (max - min) / (1 + (x/IC_{50}) ^ (Hillslope))$, where x refers to the concentration
520 of blockers, y refers to the normalized current at a certain concentration, and $IC_{50}$ is
521 the concentration that generates half of the maximal inhibition.
522

523 **Single-channel recordings**

524 Cell-attached recordings were carried out using *ltk-* mouse fibroblast cells as
525 previously described (Eldstrom, Wang, Werry, Wong, & Fedida, 2015; Murray et al.,
526 2016; Westhoff, Eldstrom, Murray, Thompson, & Fedida, 2019). Briefly, cells were
527 transfected using Lipofectamine 2000 (Invitrogen, Carlsbad, CA, USA) as per the
528 manufactures protocol, with DNA ratios of 1:0.8 of Kir3.2 G156S:GFP in micrograms.
529 Transfected cells were grown in MEM with 10% FBS (GIBCO, USA), overnight in 5%
530 $CO_2$ at 37°C. All recordings were made at room temperature, ~24 hrs post
531 transfection. The bath solution contained (mM): 135 KCl, 10 HEPES, 1 $MgCl_2$, 10
532 Dextrose, 0.05 $CaCl_2$ and was adjusted to pH 7.4 with KOH. The patch pipette
533 solution contained (mM): 10 HEPES, 1 $MgCl_2$, 10 Dextrose and either 135 KCl or 135
534 LiCl pH'ed to 7.4 with KOH or LiOH or a 50% mixture of each of these solutions.
535 Single channel recordings were made using an Axopatch 200B amplifier, Digidata
536 1330 and pClamp 9 software (Molecular Devices). Patch electrodes were pulled
537 from thick-walled borosilicate glass (Sutter Instruments, Novato, CA, USA). After fire
538 polishing and Sylgard (Dow Corning, Midland, MI, USA) application, electrode
539 resistances were between 40 and 60 MΩ. Records were sampled at 10 kHz and
540 low-pass filtered at 2 kHz using a -3dB, four-pole Bessel filter. For presentation and
541 analysis, the data was additionally filtered digitally at 200 Hz. Data was analyzed
542 with pClamp 10 (Molecular Devices) and Figures prepared using Prism 9 GraphPad
543 software (San Diego, CA, USA).

544

545 **Data and statistical analysis**

546 All statistical analyses were performed with SigmaPlot 14 (Hulinks, Japan). Data
547 shown in all Figures are means ± SD from n single cells specified in the legend of
548 each Figure. Statistical differences were evaluated using Tukey's test following one-
549 way ANOVA to compare the values between the absence or presence of pore

550 blockers with the extracellular solution containing different cations in Figure 2, 3, 6, 7
551 and SI appendix, Figure. S1. Unpaired Student's *t* test was used for Figures 3i, 3j
552 and 4e.
553
554 **Reagents**
555 Tertiapin-Q (TPN-Q) was purchased from Abcam (Cambridge, UK) or Bio-Techne
556 Canada (Toronto, Canada). ACh, Ivermectin (IVM), and the other reagents were
557 purchased from Sigma-Aldrich (St. Louis, USA), unless otherwise specified. TPN-Q
558 and ACh were dissolved in distilled water, and IVM was dissolved in DMSO. These
559 reagents were diluted to a final concentration in the extracellular solution and the
560 solvent concentration was ≤ 0.3%.
561
562 **Acknowledgments and funding sources**
563 We thank Ms. Chizue Naito, Ms. Tomomi Yamamoto and Fariba Ataei for technical
564 assistance, members in Kubo Lab for discussion, and Dr. Eitan Reuveny and Dr.
565 Izhar Karbat (Weizmann Institute of Science) for information exchange and
566 discussion. I-S. C. thanks Dr. Tomoe Y. Nakamura (Wakayama Medical University)
567 for support. This work was supported by JSPS KAKENHI Grant Numbers
568 JP20K07304 (to I-S.C.) and JP20H03424 (to Y.K.), The Uehara Memorial
569 Foundation (to I-S.C.), and grants PJT-156181 from the CIHR (to D.F.) and G-20-
570 0028720 from the Heart and Stroke Foundation of Canada (to D.F.).
571 **Author Contributions:** I-S.C. and Y.K. designed the study; I-S.C. performed all
572 experiments using *Xenopus* oocytes and data analyses. J.E. performed single
573 channel recordings and J.E. and D.F. analyzed and interpreted the data. All authors
574 wrote the paper and confirmed the final version.
575 **Competing Interest Statement:** The authors declare no conflict of interest.
576

577 **References**

578


579 Alagem, N., Dvir, M., & Reuveny, E. (2001). Mechanism of Ba(2+) block of a mouse inwardly
580 rectifying K+ channel: differential contribution by two discrete residues. *J Physiol,*
581 *534*(Pt. 2), 381-393. doi:10.1111/j.1469-7793.2001.00381.x
582 Bichet, D., Grabe, M., Jan, Y. N., & Jan, L. Y. (2006). Electrostatic interactions in the channel
583 cavity as an important determinant of potassium channel selectivity. *Proc Natl Acad*
584 *Sci U S A, 103*(39), 14355-14360. doi:10.1073/pnas.0606660103
585 Bichet, D., Lin, Y. F., Ibarra, C. A., Huang, C. S., Yi, B. A., Jan, Y. N., & Jan, L. Y. (2004). Evolving
586 potassium channels by means of yeast selection reveals structural elements
587 important for selectivity. *Proc Natl Acad Sci U S A, 101*(13), 4441-4446.
588 doi:10.1073/pnas.0401195101
589 Boulkroun, S., Beuschlein, F., Rossi, G. P., Golib-Dzib, J. F., Fischer, E., Amar, L., . . . Zennaro,
590 M. C. (2012). Prevalence, clinical, and molecular correlates of KCNJ5 mutations in
591 primary aldosteronism. *Hypertension, 59*(3), 592-598.
592 doi:10.1161/HYPERTENSIONAHA.111.186478
593 Chen, I. S., & Kubo, Y. (2018). Ivermectin and its target molecules: shared and unique
594 modulation mechanisms of ion channels and receptors by ivermectin. *J Physiol,*
595 *596*(10), 1833-1845. doi:10.1113/JP275236
596 Chen, I. S., Liu, C., Tateyama, M., Karbat, I., Uesugi, M., Reuveny, E., & Kubo, Y. (2019). Non-
597 sedating antihistamines block G-protein-gated inwardly rectifying K(+) channels. *Br J*
598 *Pharmacol, 176*(17), 3161-3179. doi:10.1111/bph.14717
599 Chen, I. S., Tateyama, M., Fukata, Y., Uesugi, M., & Kubo, Y. (2017). Ivermectin activates GIRK
600 channels in a PIP2 -dependent, Gbetagamma -independent manner and an amino
601 acid residue at the slide helix governs the activation. *J Physiol, 595*(17), 5895-5912.
602 doi:10.1113/JP274871
603 Choi, M., Scholl, U. I., Yue, P., Bjorklund, P., Zhao, B., Nelson-Williams, C., . . . Lifton, R. P.
604 (2011). K+ channel mutations in adrenal aldosterone-producing adenomas and
605 hereditary hypertension. *Science, 331*(6018), 768-772. doi:10.1126/science.1198785
606 Doupnik, C. A., Parra, K. C., & Guida, W. C. (2015). A computational design approach for
607 virtual screening of peptide interactions across K(+) channel families. *Comput Struct*
608 *Biotechnol J, 13*, 85-94. doi:10.1016/j.csbj.2014.11.004
609 Doyle, D. A., Morais Cabral, J., Pfuetzner, R. A., Kuo, A., Gulbis, J. M., Cohen, S. L., . . .
610 MacKinnon, R. (1998). The structure of the potassium channel: molecular basis of K+
611 conduction and selectivity. *Science, 280*(5360), 69-77.
612 doi:10.1126/science.280.5360.69
613 Eisenman, G. (1962). Cation selective glass electrodes and their mode of operation. *Biophys*
614 *J, 2*(2 Pt 2), 259-323. doi:10.1016/s0006-3495(62)86959-8
615 Eldstrom, J., Wang, Z., Werry, D., Wong, N., & Fedida, D. (2015). Microscopic mechanisms for
616 long QT syndrome type 1 revealed by single-channel analysis of I(Ks) with S3 domain
617 mutations in KCNQ1. *Heart Rhythm, 12*(2), 386-394.
618 doi:10.1016/j.hrthm.2014.10.029
619 Guo, R., Zeng, W., Cui, H., Chen, L., & Ye, S. (2014). Ionic interactions of Ba2+ blockades in
620 the MthK K+ channel. *J Gen Physiol, 144*(2), 193-200. doi:10.1085/jgp.201411192
621 Heginbotham, L., Lu, Z., Abramson, T., & MacKinnon, R. (1994). Mutations in the K+ channel
622 signature sequence. *Biophys J, 66*(4), 1061-1067. doi:10.1016/S0006-
623 3495(94)80887-2

Hibino, H., Inanobe, A., Furutani, K., Murakami, S., Findlay, I., & Kurachi, Y. (2010). Inwardly rectifying potassium channels: their structure, function, and physiological roles. *Physiol Rev, 90*(1), 291-366. doi:10.1152/physrev.00021.2009

Hille, B. (2001). Sinauer Associates Inc.

Horvath, G. A., Zhao, Y., Tarailo-Graovac, M., Boelman, C., Gill, H., Shyr, C., . . . van Karnebeek, C. D. M. (2018). Gain-of-function KCNJ6 Mutation in a Severe Hyperkinetic Movement Disorder Phenotype. *Neuroscience, 384*, 152-164. doi:10.1016/j.neuroscience.2018.05.031

Hsieh, C. P., Kuo, C. C., & Huang, C. W. (2015). Driving force-dependent block by internal Ba(2+) on the Kir2.1 channel: Mechanistic insight into inward rectification. *Biophys Chem, 202*, 40-57. doi:10.1016/j.bpc.2015.04.003

Kofuji, P., Hofer, M., Millen, K. J., Millonig, J. H., Davidson, N., Lester, H. A., & Hatten, M. E. (1996). Functional analysis of the weaver mutant GIRK2 K+ channel and rescue of weaver granule cells. *Neuron, 16*(5), 941-952. doi:10.1016/s0896-6273(00)80117-8

Krapivinsky, G., Gordon, E. A., Wickman, K., Velimirovic, B., Krapivinsky, L., & Clapham, D. E. (1995). The G-protein-gated atrial K+ channel IKACh is a heteromultimer of two inwardly rectifying K(+)-channel proteins. *Nature, 374*(6518), 135-141. doi:10.1038/374135a0

Kubo, Y., Reuveny, E., Slesinger, P. A., Jan, Y. N., & Jan, L. Y. (1993). Primary structure and functional expression of a rat G-protein-coupled muscarinic potassium channel. *Nature, 364*(6440), 802-806. doi:10.1038/364802a0

Lesage, F., Duprat, F., Fink, M., Guillemare, E., Coppola, T., Lazdunski, M., & Hugnot, J. P. (1994). Cloning provides evidence for a family of inward rectifier and G-protein coupled K+ channels in the brain. *FEBS Lett, 353*(1), 37-42. doi:10.1016/0014-5793(94)01007-2

Long, S. B., Campbell, E. B., & Mackinnon, R. (2005). Crystal structure of a mammalian voltage-dependent Shaker family K+ channel. *Science, 309*(5736), 897-903. doi:10.1126/science.1116269

Maiolino, G., Ceolotto, G., Battistel, M., Barbiero, G., Cesari, M., Amar, L., . . . Rossi, G. P. (2018). Macrolides for KCNJ5-mutated aldosterone-producing adenoma (MAPA): design of a study for personalized diagnosis of primary aldosteronism. *Blood Press, 27*(4), 200-205. doi:10.1080/08037051.2018.1436961

Masotti, A., Uva, P., Davis-Keppen, L., Basel-Vanagaite, L., Cohen, L., Pisaneschi, E., . . . Dallapiccola, B. (2015). Keppen-Lubinsky syndrome is caused by mutations in the inwardly rectifying K+ channel encoded by KCNJ6. *Am J Hum Genet, 96*(2), 295-300. doi:10.1016/j.ajhg.2014.12.011

Matamoros, M., & Nichols, C. G. (2021). Pore-forming transmembrane domains control ion selectivity and selectivity filter conformation in the KirBac1.1 potassium channel. *J Gen Physiol, 153*(5). doi:10.1085/jgp.202012683

Miller, A. N., & Long, S. B. (2012). Crystal structure of the human two-pore domain potassium channel K2P1. *Science, 335*(6067), 432-436. doi:10.1126/science.1213274

Murray, C. I., Westhoff, M., Eldstrom, J., Thompson, E., Emes, R., & Fedida, D. (2016). Unnatural amino acid photo-crosslinking of the IKs channel complex demonstrates a KCNE1:KCNQ1 stoichiometry of up to 4:4. *Elife, 5*. doi:10.7554/eLife.11815

Navarro, B., Kennedy, M. E., Velimirovic, B., Bhat, D., Peterson, A. S., & Clapham, D. E. (1996). Nonselective and G betagamma-insensitive weaver K+ channels. *Science, 272*(5270), 1950-1953. doi:10.1126/science.272.5270.1950

Patel, D., Kuyucak, S., & Doupnik, C. A. (2020). Structural Determinants Mediating Tertiapin Block of Neuronal Kir3.2 Channels. *Biochemistry, 59*(7), 836-850. doi:10.1021/acs.biochem.9b01098

Patil, N., Cox, D. R., Bhat, D., Faham, M., Myers, R. M., & Peterson, A. S. (1995). A potassium channel mutation in weaver mice implicates membrane excitability in granule cell differentiation. *Nat Genet, 11*(2), 126-129. doi:10.1038/ng1095-126

Prutting, S., & Grissmer, S. (2011). A novel current pathway parallel to the central pore in a mutant voltage-gated potassium channel. *J Biol Chem, 286*(22), 20031-20042. doi:10.1074/jbc.M110.185405

Roy, R. N., Hendriks, K., Kopec, W., Abdolvand, S., Weiss, K. L., de Groot, B. L., . . . Coates, L. (2021). Structural plasticity of the selectivity filter in a nonselective ion channel. *IUCrJ, 8*(Pt 3), 421-430. doi:10.1107/S205225252100213X

Scholl, U. I., Abriola, L., Zhang, C., Reimer, E. N., Plummer, M., Kazmierczak, B. I., . . . Lifton, R. P. (2017). Macrolides selectively inhibit mutant KCNJ5 potassium channels that cause aldosterone-producing adenoma. *J Clin Invest, 127*(7), 2739-2750. doi:10.1172/JCI91733

Scholl, U. I., Nelson-Williams, C., Yue, P., Grekin, R., Wyatt, R. J., Dillon, M. J., . . . Lifton, R. P. (2012). Hypertension with or without adrenal hyperplasia due to different inherited mutations in the potassium channel KCNJ5. *Proc Natl Acad Sci U S A, 109*(7), 2533-2538. doi:10.1073/pnas.1121407109

Shi, C., He, Y., Hendriks, K., de Groot, B. L., Cai, X., Tian, C., . . . Sun, H. (2018). A single NaK channel conformation is not enough for non-selective ion conduction. *Nat Commun, 9*(1), 717. doi:10.1038/s41467-018-03179-y

Slesinger, P. A., Patil, N., Liao, Y. J., Jan, Y. N., Jan, L. Y., & Cox, D. R. (1996). Functional effects of the mouse weaver mutation on G protein-gated inwardly rectifying K+ channels. *Neuron, 16*(2), 321-331. doi:10.1016/s0896-6273(00)80050-1

Tyutyaev, P., & Grissmer, S. (2017). Observation of sigma-pore currents in mutant hKv1.2_V370C potassium channels. *PLoS One, 12*(4), e0176078. doi:10.1371/journal.pone.0176078

Tyutyaev, P., & Grissmer, S. (2018). Characterization of the sigma-Pore in Mutant hKv1.3 Potassium Channels. *Cell Physiol Biochem, 46*(3), 1112-1121. doi:10.1159/000488840

Velarde-Miranda, C., Gomez-Sanchez, E. P., & Gomez-Sanchez, C. E. (2013). Regulation of aldosterone biosynthesis by the Kir3.4 (KCNJ5) potassium channel. *Clin Exp Pharmacol Physiol, 40*(12), 895-901. doi:10.1111/1440-1681.12151

Wang, S., Lee, S. J., Maksaev, G., Fang, X., Zuo, C., & Nichols, C. G. (2019). Potassium channel selectivity filter dynamics revealed by single-molecule FRET. *Nat Chem Biol, 15*(4), 377-383. doi:10.1038/s41589-019-0240-7

Wang, W., & MacKinnon, R. (2017). Cryo-EM Structure of the Open Human Ether-a-go-go-Related K(+) Channel hERG. *Cell, 169*(3), 422-430 e410. doi:10.1016/j.cell.2017.03.048

Westhoff, M., Eldstrom, J., Murray, C. I., Thompson, E., & Fedida, D. (2019). I Ks ion-channel pore conductance can result from individual voltage sensor movements. *Proc Natl Acad Sci U S A, 116*(16), 7879-7888. doi:10.1073/pnas.1811623116

Whorton, M. R., & MacKinnon, R. (2011). Crystal structure of the mammalian GIRK2 K+ channel and gating regulation by G proteins, PIP2, and sodium. *Cell, 147*(1), 199-208. doi:10.1016/j.cell.2011.07.046

Yang, J., Yu, M., Jan, Y. N., & Jan, L. Y. (1997). Stabilization of ion selectivity filter by pore loop ion pairs in an inwardly rectifying potassium channel. *Proc Natl Acad Sci U S A, 94*(4), 1568-1572. doi:10.1073/pnas.94.4.1568

Yi, B. A., Lin, Y. F., Jan, Y. N., & Jan, L. Y. (2001). Yeast screen for constitutively active mutant G protein-activated potassium channels. *Neuron, 29*(3), 657-667. doi:10.1016/s0896-6273(01)00241-0

Zagotta, W. N. (2006). Membrane biology: permutations of permeability. *Nature, 440*(7083), 427-429. doi:10.1038/440427a

Zangerl-Plessl, E. M., Qile, M., Bloothooft, M., Stary-Weinzinger, A., & van der Heyden, M. A. G. (2019). Disease Associated Mutations in KIR Proteins Linked to Aberrant Inward Rectifier Channel Trafficking. *Biomolecules, 9*(11). doi:10.3390/biom9110650

Zhou, Y., Morais-Cabral, J. H., Kaufman, A., & MacKinnon, R. (2001). Chemistry of ion coordination and hydration revealed by a K+ channel-Fab complex at 2.0 A resolution. *Nature, 414*(6859), 43-48. doi:10.1038/35102009

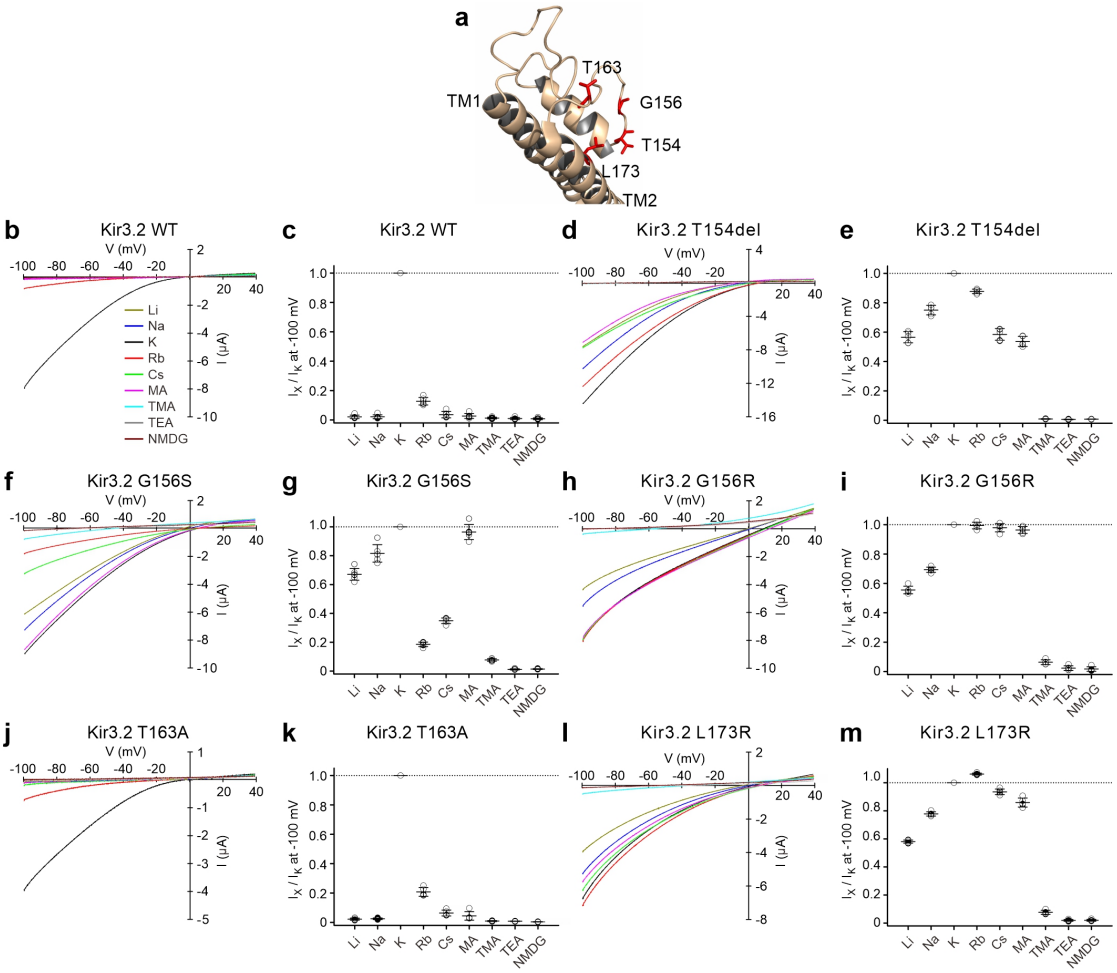


**Figure 1. Permeation of various cations in inherited Kir3.2 mutants expressed in *Xenopus* oocytes**

(**a**) The crystal structure of the pore-forming region of Kir3.2 WT (Protein Data Bank ID: 3SYA)(Whorton & MacKinnon, 2011). The positions of inherited mutations are shown and labelled in red in stick mode. The IV-relationship of Kir3.2 WT (**b**), T154del (**d**), G156S (**f**), G156R (**h**), T163A (**j**), and L173R (**l**) were recorded by a ramp pulse from -100 mV to +40 mV for 1 s in an extracellular solution containing 96 mM XCl, where the X is Li, Na, K, Rb, Cs, MA, TMA, TEA, or NMDG, respectively. (**c**, **e**, **g**, **i**, **k**, **m**) The current amplitude of $X^+$ relative to $K^+$ ($I_X/I_K$) of each mutant at -100 mV was calculated by normalization of $I_K$ as 1. Data shown are individual values with means ± SD, n = 6 for WT and G156S; n = 5 for the other mutants.

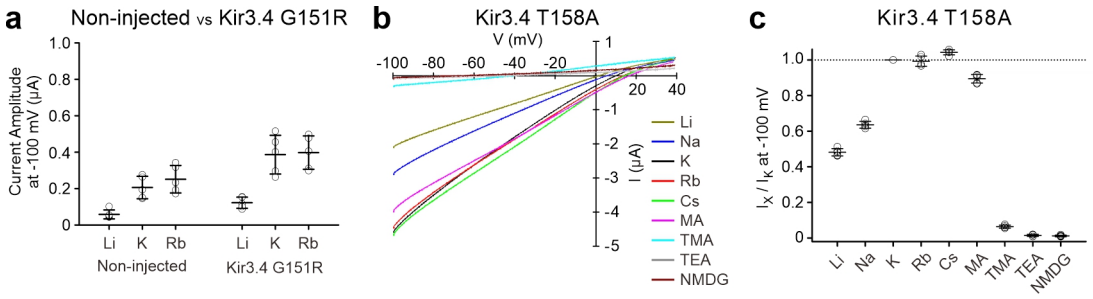


**Figure 1-figure supplement 1. Permeation of various cations in Kir3.4 G151R and Kir3.4 T158A expressed in *Xenopus* oocytes**

(**a**) The current amplitude recorded from the oocytes without injection of cRNA or injected with cRNA of Kir3.4 G151R at -100 mV in the extracellular solution containing 96 mM LiCl, KCl, or RbCl, respectively. (**b**) The IV-relationship of Kir3.4 T158A with different cations in the extracellular solution. (**c**) The current amplitude of $X^+$ relative to $K^+$ ($I_X/I_K$) of each cation was calculated by normalization of $I_K$ as 1. Data shown are individual values with means ± SD, n = 5.

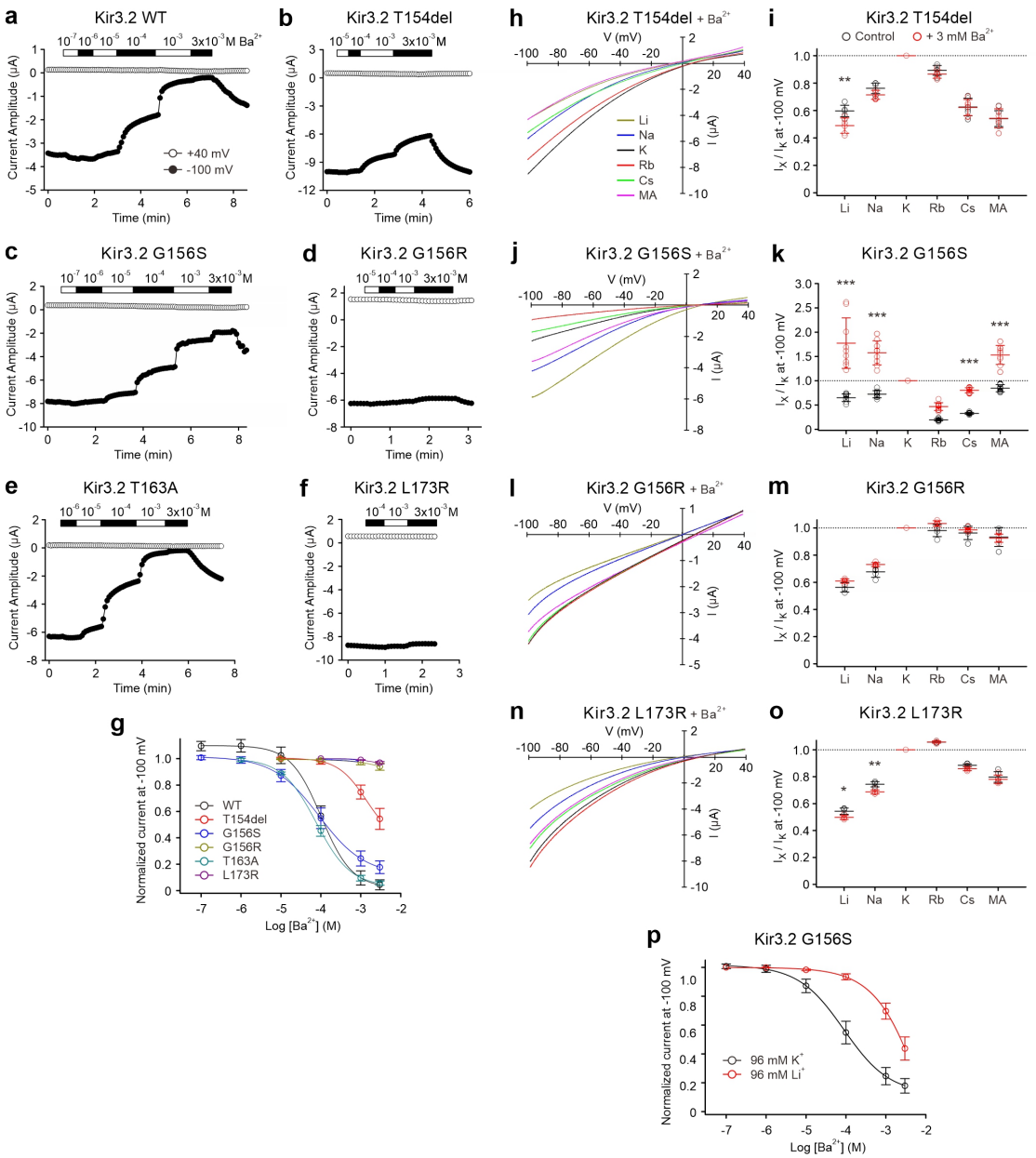


**Figure 2. Effect of $Ba^{2+}$ on the current of various cations in inherited Kir3.2 mutants expressed in *Xenopus* oocytes**

(**a-f**) Representative time course of current change of Kir3.2 WT and mutants at -100 mV and +40 mV before and after applications of different concentrations of $BaCl_2$ in the extracellular solution. (**g**) Dose-inhibition relationship at -100 mV. Data shown are means ± SD, n = 5 for each. The IV-relationship of Kir3.2 T154del (**h**), G156S (**j**), G156R (**l**), and L173R (**n**) were recorded by a ramp pulse from -100 mV to +40 mV for 1 s in an extracellular solution containing 96 mM XCl, where the X refers to Li, Na,

765 K, Rb, Cs, or MA, respectively (**i**, **k**, **m**, **o**). The $I_X/I_K$ of each mutant at -100 mV before
766 (black symbols) and after the application of 3 mM $BaCl_2$ (red symbols). Data shown
767 are individual values with means ± SD, n = 6 for T154del; n = 9 for G156S; n = 5 for
768 the other mutants. * $P < 0.05$, ** $P < 0.01$, *** $P < 0.001$ depict the significance of
769 statistical difference between the values in the absence and the presence of $Ba^{2+}$. (**p**)
770 Dose-inhibition relationship of $Ba^{2+}$ on the $K^+$ current (black symbols) or the $Li^+$
771 current (red symbols) of Kir3.2 G156S, means ± SD, n = 5 for each.
772

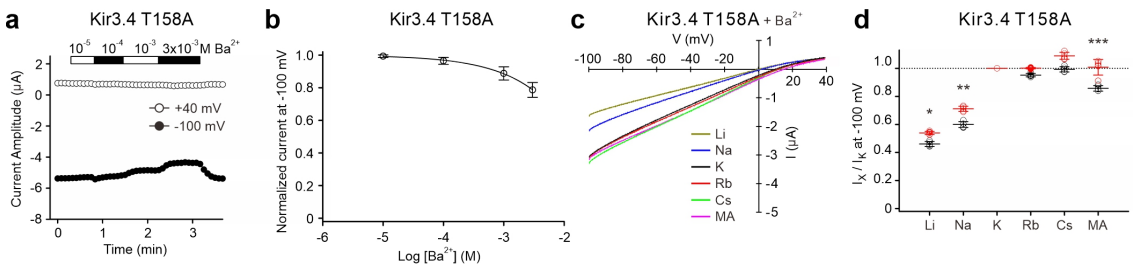


773

774 **Figure 2-figure supplement 1. Effect of $Ba^{2+}$ on the current of Kir3.4 T158A**

775 **expressed in *Xenopus* oocytes**

776 (**a**) Time course of current change of oocytes expressed Kir3.4 T158A at -100 mV

777 and +40 mV before and after applications of different concentrations of $Ba^{2+}$ in the 96

778 mM KCl extracellular solution. (**b**) Dose-inhibition relationship of $Ba^{2+}$ on $K^+$ current,

779 means ± SD, n = 5. (**c**) The IV-relationship of Kir3.4 T158A in the presence of 3 mM

780 $Ba^{2+}$. (**d**) The $I_X/I_K$ at -100 mV before (black symbols) and after the application of 3

781 mM $Ba^{2+}$ (red symbols), means ± SD, n = 5. * $P < 0.05$, ** $P < 0.01$, *** $P < 0.001$

782 depict the statistical significance of the difference between the absence and the

783 presence of $Ba^{2+}$.

784

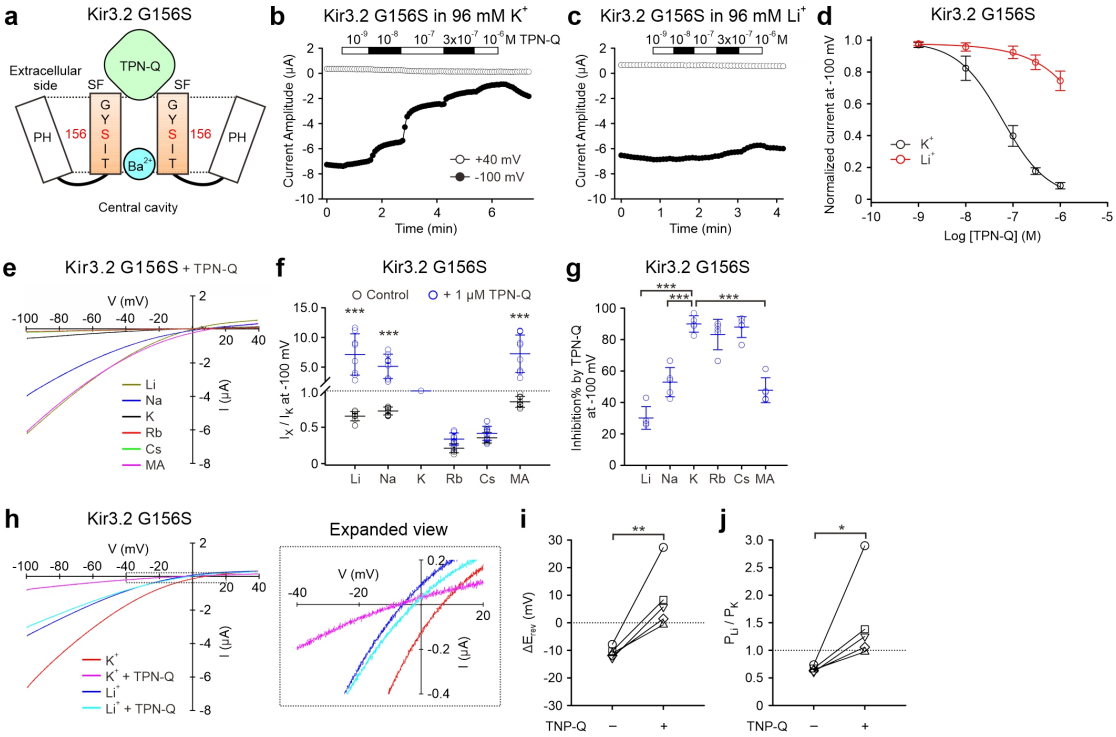


**Figure 3. Effect of TPN-Q on the current of various cations of Kir3.2 G156S expressed in *Xenopus* oocytes**

(**a**) A schematic drawing of the pore-forming region and the location of G156S of Kir3.2. $Ba^{2+}$ and TPN-Q block the ion permeation route formed by the SF are drawn according to previous studies (Alagem et al., 2001; Doupnik et al., 2015; Hsieh et al., 2015; Patel et al., 2020). Time course of current change at -100 mV and +40 mV before and after applications of different concentrations of TPN-Q in the extracellular solution containing 96 mM KCl (**b**) or LiCl (**c**). (**d**) Dose-inhibition relationship of $K^+$ current (black symbols) and $Li^+$ current (red symbols) at -100 mV, means ± SD, n = 5 for each. (**e**) The IV-relationship of each cation in the presence of 1 μM TPN-Q. (**f**) The $I_X/I_K$ at -100 mV before (black symbols) and after the application of TPN-Q (blue symbols). Data shown are individual values with means ± SD, n = 8. *** $P < 0.001$ depict the statistical significance of difference between the absence and the presence of TPN-Q. (**g**) Inhibition percentage of cation currents at -100 mV by 1 μM TPN-Q, means ± SD, n = 5 for each, *** $P < 0.001$ as compared the $K^+$ group. (**h**) The IV-relationship of $K^+$ and $Li^+$ current in the absence or presence of 1 μM TPN-Q.

802 An expanded view of zero current range is shown in the right panel. (**i**) The shift of
803 reversal potential when the extracellular $Li^+$ was replaced with $K^+$, means ± SD, n = 5.
804 (**j**) The permeability of $Li^+$ relative to the permeability of $K^+$ ($P_{Li}/P_K$) were calculated
805 from (**i**), means ± SD, n = 5. * $P < 0.05$, ** $P < 0.01$ depict the statistical significance
806 of difference between the values in the absence and the presence of TPN-Q.
807

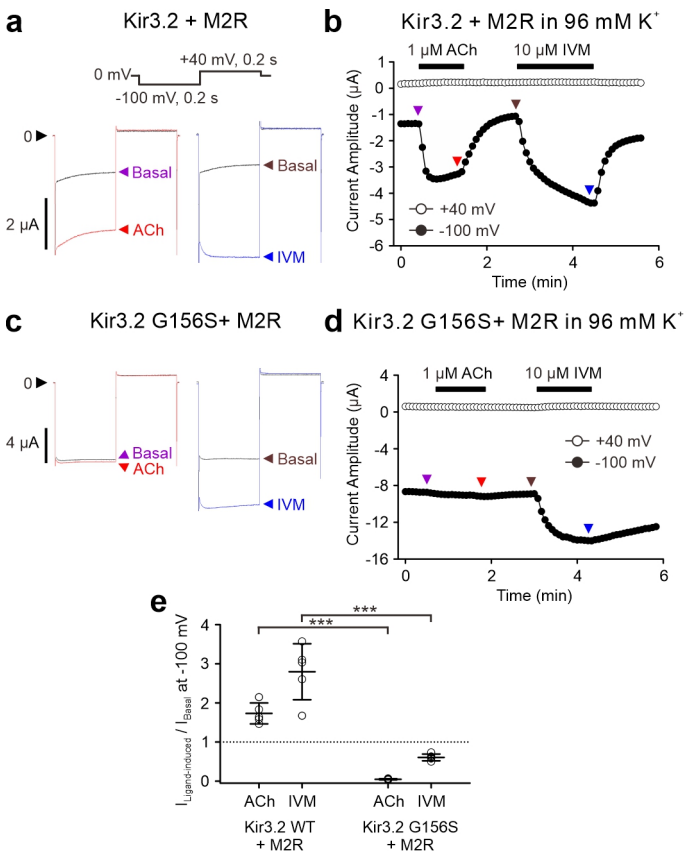


808

809 **Figure 4. Effects of activators of GIRK channels on the current of Kir3.2 G156S**

810 **expressed in *Xenopus* oocytes**

811 Current of oocytes expressing Kir3.2 WT with M2R (**a**, **b**) or Kir3.2 G156S with M2R

812 (**c**, **d**) were recorded in an extracellular solution containing 96 mM $K^+$ with a protocol

813 shown above. Current traces before or after the application of 1 μM ACh or 10 μM

814 Ivermectin (IVM) at the time indicated by arrows (**b**, **d**) are shown in (**a**, **c**). (**e**) The

815 amplitudes of ACh-induced current or IVM-induced current ($I_{Ligand\text{-}induced}$) relative to the

816 basal currents ($I_{Basal}$) were calculated by normalization of $I_{Basal}$ as 1. Data shown are

817 individual values with means ± SD, n = 5 for each. *** $P < 0.001$ indicates the

818 statistical significance of the difference between the WT and the mutant.

819

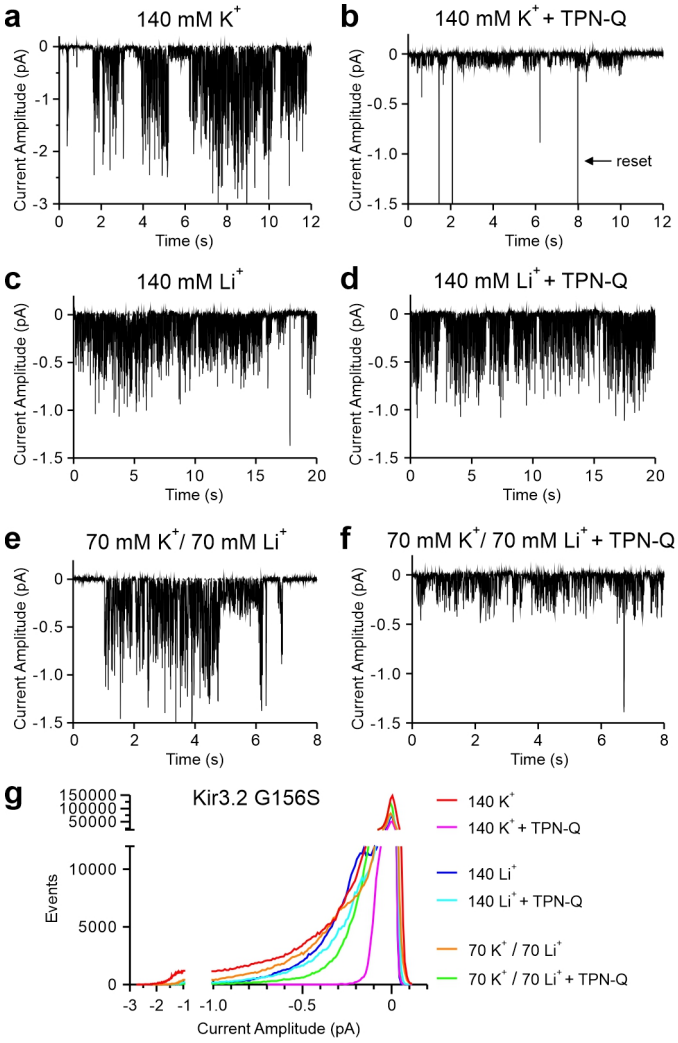


**Figure 5. Single-channel activity of Kir3.2 G156S mutant expressed in mouse fibroblasts**

Representative single channel recordings of the Kir3.2 G156S mutant at -100 mV with 140 mM $K^+$ (**a**, **b**), 140 mM $Li^+$ (**c**, **d**) or a mixture or 70 mM $K^+$/70 mM $Li^+$ (**e**, **f**) in the recording pipette, with or without 400 nM TPN-Q as indicated. Occasional artifacts due to amplifier resets are unavoidable and an example is indicated in (**b**). (**g**) Current amplitude histograms of net ion conduction events in the absence or presence of TPN-Q with three types of solution compositions. Data are pooled from n = 3 to 5 for each condition.

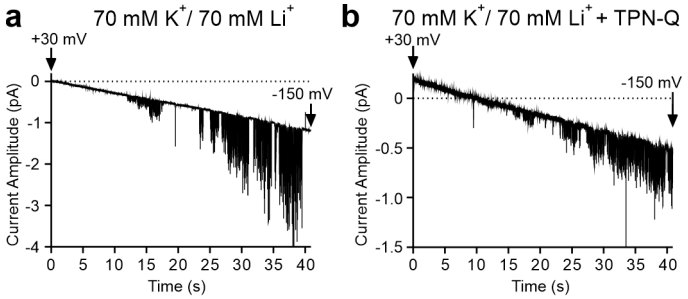


**Figure 5-figure supplement 1. The voltage-conductance relationship of Kir3.2 G156S expressed in mouse fibroblasts**

Single-channel recordings of Kir3.2 G156S were recorded with pipette solution containing 70 mM $K^+$ and 70 mM $Li^+$ in the absence (**a**) or presence of 400 nM TPN-Q (**b**) with a ramp pulse from +30 mV to -150 mV for 40 s.

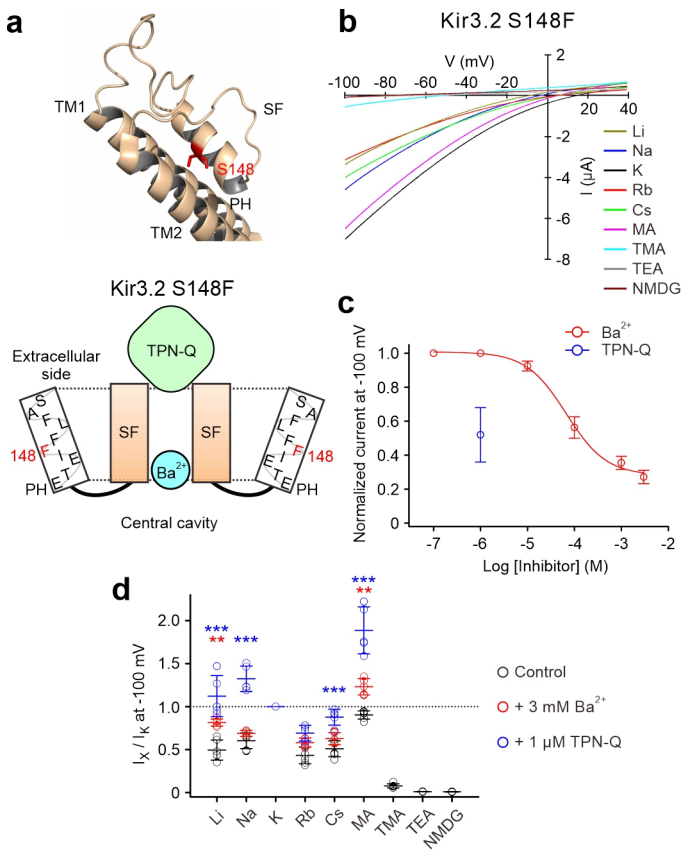


**Figure 6. Permeation of various cations and the effect of blockers on the currents of Kir3.2 S148F expressed in *Xenopus* oocytes**

(**a**) The position of S148 (labelled in red) at the pore helix (PH) of Kir3.2 WT. (**b**) The IV-relationship of each cation. (**c**) Dose-inhibition relationship of $Ba^{2+}$ (red symbols) and TPN-Q (blue symbols) on $K^+$ current at -100 mV, means ± SD, n = 5 for each. (**d**) The $I_X/I_K$ at -100 mV in the absence of blocker (black symbols), and in the presence of 3 mM $Ba^{2+}$ (red symbols) or 1 μM TPN-Q (blue symbols). Data shown are individual values with means ± SD, n = 6 for control group; n = 5 for the other groups. ** $P < 0.01$, *** $P < 0.001$ depict the statistical significance of difference between the absence and the presence of $Ba^{2+}$ (red *) or TPN-Q (blue *).

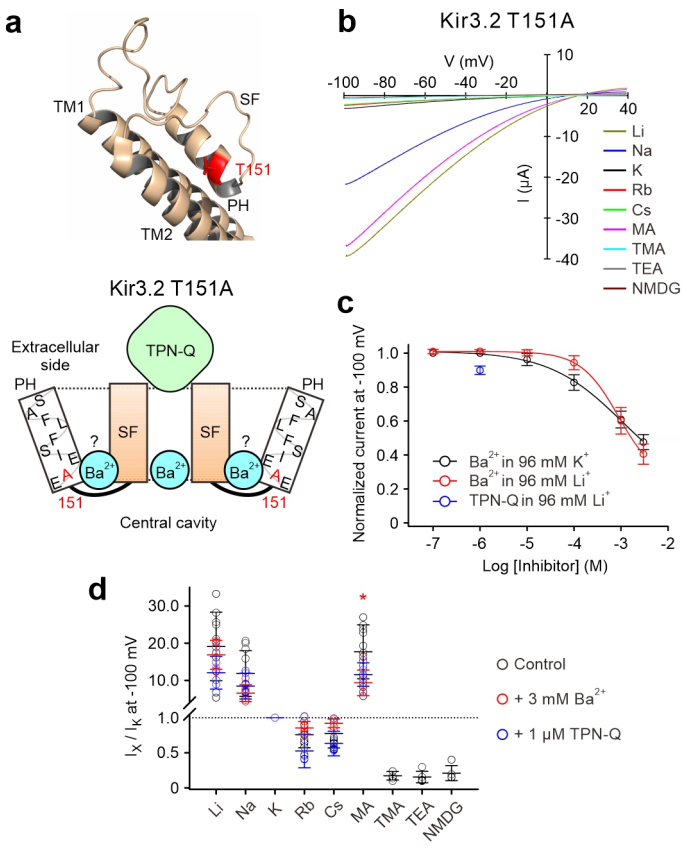


**Figure 7. Permeation of various cations and the effect of blockers on the currents of Kir3.2 T151A expressed in *Xenopus* oocytes**

(**a**) The position of T151A (labelled in red) in the pore helix of Kir3.2 WT. (**b**) The IV-relationship of each cation. (**c**) Dose-inhibition relationship of $Ba^{2+}$ on $K^+$ current (black symbols) or $Li^+$ current (red symbols), and TPN-Q on $Li^+$ current (blue symbols) at -100 mV, means ± SD, n = 5 for each. (**d**) The $I_X/I_K$ at -100 mV in the absence of blocker (black symbols), and in the presence of 3 mM $Ba^{2+}$ (red symbols) or 1 μM TPN-Q (blue symbols). Data shown are individual values with means ± SD, n = 5 to 10 for control group; n = 7 for $Ba^{2+}$ group; n = 6 for TPN-Q group. Red * $P < 0.05$ depict the statistical significance of the difference between the absence and the presence of $Ba^{2+}$. There were no significant differences between the absence and presence of TPN-Q are shown.

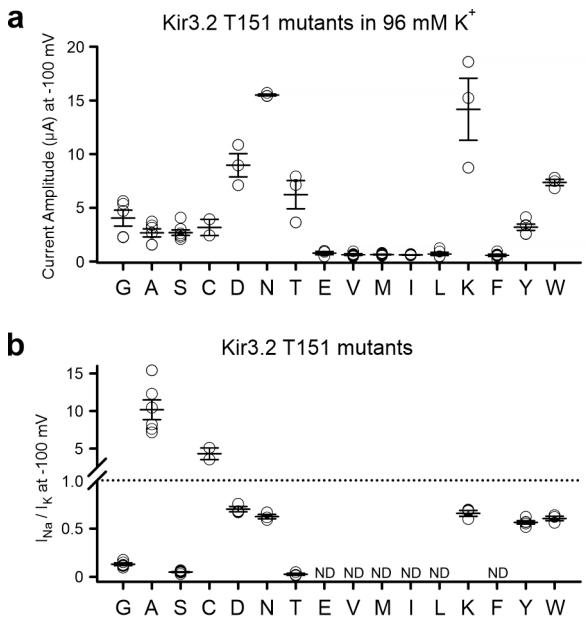


**Figure 7-figure supplement 1. The current amplitude and the ion selectivity of various Kir3.2 mutants at T151 expressed in *Xenopus* oocytes.**

(**a**) The basal current amplitude of Kir3.2 T151 mutants at -100 mV in the 96 mM KCl extracellular solution. (**b**) The $I_{Na}/I_K$ of Kir3.2 T151 mutants at -100 mV. All data shown are means ± SD, n = 5 for T151G, V, L, F, Y; n = 6 for T151A, I; n = 7 for T151S; n = 8 for T151M; n = 2 for T151C; n = 3 for other mutants. The $I_{Na}/I_K$ of T151E, V, M, I, L, F mutants is not detectable (indicated as ND) because of their very small current amplitudes as shown in (**a**).

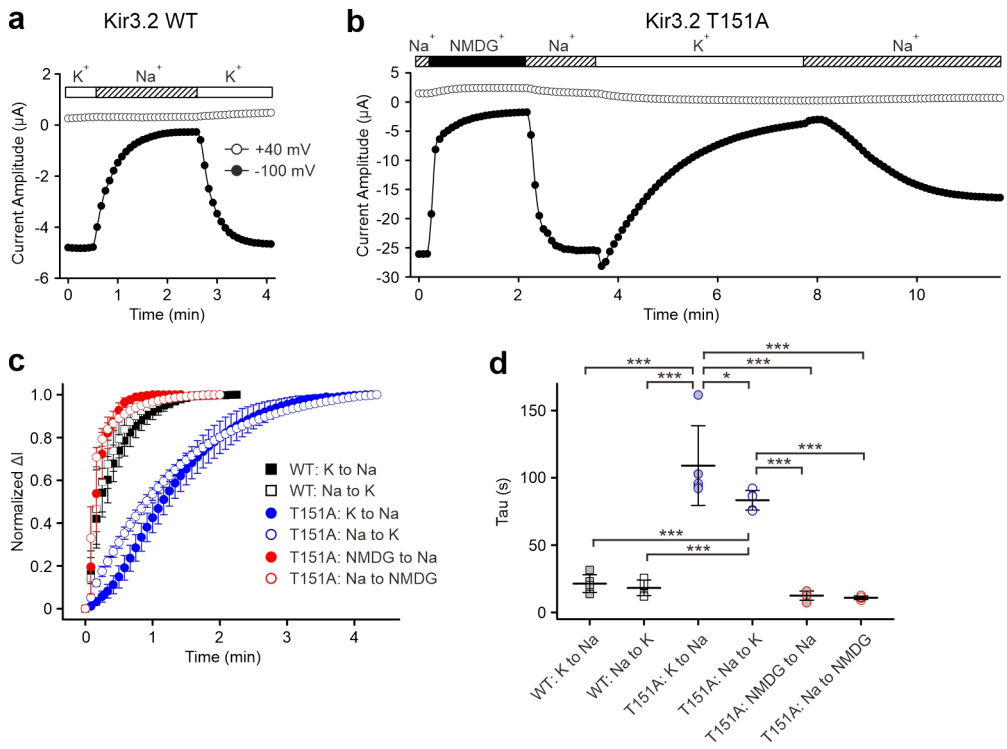


**Figure 7-figure supplement 2. The kinetics of current amplitude change of Kir3.2 T151A upon exchange of extracellular cations.**

(**a, b**) Representative time course of current amplitude change of Kir3.2 WT (**a**) and Kir3.2 T151A mutant (**b**) at -100 mV and +40 mV during the exchange of extracellular solution with 96 mM $K^+$ or $Na^+$ or $NMDG^+$ as shown above. (**c**) The kinetics of current amplitude change upon the exchange of extracellular cations calculated from the current amplitude at -100 mV. The maximal difference of current amplitude before and after replacement of extracellular solution was normalized to 1. Data shown are means ± SD, n = 5 for each. (**d**) Tau of current amplitude change, means ± SD, n = 5 for each. * $P < 0.05$, *** $P < 0.001$ depict the statistical significance.